*Journal of The Electrochemical Society*, **149** (9) A1196-A1200 (2002)
0013-4651/2002/149(9)/A1196/5/$7.00 © The Electrochemical Society, Inc.

# Investigation of the Lithium Couple on Pt, Al, and Hg Electrodes in Lithium Imide-Ethyl Methyl Sulfone

**Sea H. Park,* Jack Winnick,** and Paul A. Kohl**,z**

*School of Chemical Engineering, Georgia Institute of Technology, Atlanta, Georgia 30332-0100, USA*

The electrochemical behavior of lithium bis(trifluoromethanesulfonyl)imide in ethyl methyl sulfone was studied. The coulombic efficiencies for the oxidation-reduction of lithium at platinum, aluminum, and mercury electrodes were 50, 93, and 99%, respectively. A comparison of the results with Pt, Al, and Hg electrodes suggests that chemical reactions of lithium with the electrolyte contribute to the efficiency loss with the Pt and Al electrodes. Low coulombic efficiencies for lithium on the Pt substrate were due to chemical reactions involving elemental lithium and the low reduction-oxidation reversibility of the lithium in Li-Pt alloys. For the Al substrate, the chemical reactions produced protective films on the surface of the Li-Al alloys. The self-discharge rate of the lithium on the Al substrate was very low, 0.3 $\mu$A/cm$^2$. The electrochemical reduction of lithium on mercury occurred at the least negative potential because of the amalgam formation. The lithium amalgam did not react with the electrolyte, resulting in the high coulombic efficiency.
 [DOI: 10.1149/1.1497979] 

Manuscript submitted November 30, 2001; revised manuscript received March 8, 2002. Available electronically August 1, 2002.

Lithium batteries are widely used for mobile electronics. A great deal of research has been carried out on the lithium metal and lithium ion batteries to improve the cyclability of the lithium electrode and suppress lithium dendrite formation.[1-3] These studies can be divided into three groups: (*i*) solvents, (*ii*) anions, and (*iii*) electrode materials. The ideal solvent would possess a low melting temperature, good conductivity, low volatility, and an electrochemical window sufficiently large to permit both the deposition of lithium and a corresponding cathode reaction. It should also suppress dendrite formation and have low reactivity toward lithium. The advantages and disadvantages of solvents and ionic liquids have been discussed.[4-8]

One figure of merit for the stability of lithium in the electrolyte is the coulombic efficiency, which is defined as a ratio of the stripping charge passed to the plating charge passed. No electrolyte has yet produced 100% coulombic efficiency for the lithium reduction/oxidation processes. Lithium readily reacts with solvents, anions, and impurities due to its high electropositive nature, resulting in loss of coulombic efficiency.[9]

Xu reported that ethyl methyl sulfone (EMSF) solvent with lithium bis(trifluoromethanesulfonyl)imide (LiTFSI) electrolyte exhibited good stability.[7] This electrolyte has a conductivity of $10^{-2.5}$ S/cm at room temperature, and the positive potential limit is 5.6 V *vs.* Li/Li$^+$.[7] A high coulombic efficiency for lithium deposition/dissolution was observed in cyclic voltammetry experiments; however loss of the charge or reactivity of EMSF toward lithium was not discussed.

Lithium imide salts are promising candidates for lithium batteries because of their low reactivity toward lithium metal, stability at ambient temperature, and high conductivity. The imide ion is larger than other anions, such as $PF_6^-$, $ClO_4^-$, $AsF_6^-$, and $BF_4^-$, which improves the conductivity and lowers the reactivity to lithium.[10]

New anode host-materials for lithium based on carbon, oxides, and alloys are being extensively investigated.[2,11-15] The lithium-aluminum alloys showed high coulombic efficiencies, but their mechanical strength was relatively low because the volume of Li-Al alloys is three times greater than aluminum alone.[2] It was suggested that less than 100% coulombic efficiency was due to loss of mechanical integrity.[2,15]

In this study, we have examined the electrochemical behavior of the LiTFSI-EMSF electrolyte with respect to the stability of the Li$^+$/Li couple, using electrochemical techniques and the electrochemical quartz crystal nanobalance (EQCN). The EQCN has been used to investigate reactions on the surface of a working electrode in the LiTFSI-EMSF electrolyte. The EQCN can be used in the controlled potential or current electrochemical experiments. The mass change on the electrode can be obtained from the Sauerbrey equation[16-19]

$$\Delta f = -\frac{2 f_0^2 \Delta m}{A(\mu_q \rho_q)^{1/2}} \quad [1]$$

where $\Delta f$ is the frequency shift, $f_0$ is the resonant frequency, $\Delta m$ is the mass change, $A$ is the piezoelectrically active area, $\mu_q$ is the shear modulus of the quartz crystal, and $\rho_q$ is the density of the quartz crystal. The mass change of the quartz crystal is directly proportional to the frequency shift. Linearity of frequency change with respect to mass change was observed from this relationship up to a certain thickness of the film deposited. Mass change can be related to charge passed according to Faraday's law.

Rate of mass change ($rmc$) was derived from the Faraday's law to compare the mass change from the EQCM to the corresponding current density. The derivative of mass with respect to time was multiplied by the Faraday constant, $F$, and divided by effective equivalent weight, $MM/n$ and then normalized to area, Eq. 2. The units on $rmc$ are current/area. The quantity was normalized to area so that it can be directly compared to the current density, which is of interest in battery applications. The effective equivalent weight ($MM/n$) was calculated from the overall mass change divided by the charge passed during either the reduction or oxidation process and multiplied by Faraday constant. The value is given for each calculation in the Results section

$$rmc = \frac{\frac{dm}{dt} \cdot F \cdot \left(\frac{n}{MM}\right)}{A} \quad [2]$$

## Experimental

Ethyl methyl sulfone was obtained from Chevron Phillips Chemical Company. It was vacuum dried at ambient temperature for 3 days. Lithium bis(trifluoromethanesulfonyl)imide [$LiN(CF_3SO_2)_2$] was obtained from 3M and was vacuum dried at 120°C for 2 days.

An EG&G model 273 potentiostat was used for cyclic voltammetry (CV) and chronoamperometry (CA). The electrodes were fabricated from 0.5 mm diam, 99.9999% pure, aluminum wire (Alfa Metals, Ashland, OR) and 99.999% pure platinum wire (ESPI, Ward Hill, MA). The working electrode was a platinum or aluminum wire and the counter electrode was a coil of platinum wire. The reference electrode was formed by immersing a lithium ribbon in the LiTFSI-

* Electrochemical Society Student Member.
** Electrochemical Society Active Member.
z E-mail: paul.kohl@che.gatech.edu

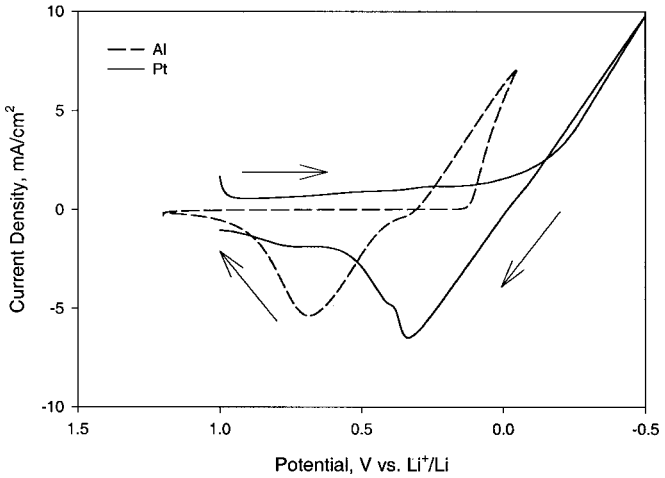


**Figure 1.** CVs of aluminum and platinum in LiTFSI-EMSF. Area of the Al WE is 0.0785 cm$^2$. Area of Pt WE is 0.158 cm$^2$.

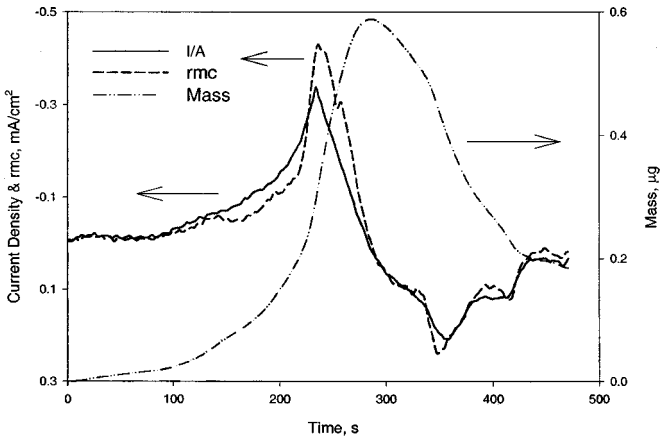


**Figure 2.** CV of platinum in LiTFSI-EMSF with mass change and *rmc*. Area of WE is 0.252 cm$^2$.

EMSF electrolyte in a glass tube sealed with a glass frit. For the mercury film electrode, gold was electroplated on the Pt wire and dipped in a mercury pool. The Hg film electrode was not used in the EQCN configuration because the mass of the Hg was too high to permit electrode vibration.

An EQCN-701 from Elchema (New York, NY) was used in the electrolyte to measure the mass of the electrodeposited lithium. The working electrode in the EQCN experiments was an AT-cut platinum-coated quartz crystal (ICM, Oklahoma City, OK) operated at 10 MHz in a Faraday cage. An EG&G bipotentiostat 366 was used with an EG&G 175 universal programmer and HP 7090A plotter. IR compensation was not used. The Al EQCN working electrode consisted of sputtered Al on the Pt quartz crystal. The area of the Al on the Pt quartz crystal was 0.384 cm$^2$.

The EQCN was calibrated for charge-to-mass deposited by electroplating copper from an acidic, aqueous copper sulfate solution. A duplicate calibration was performed by depositing silver from an acidic silver nitrate solution. The calibrations agreed to within experimental error ($\pm 2\%$).

## Results

*Investigation of Pt substrate*.—Platinum, aluminum, and mercury electrodes were used to characterize the Li/Li$^+$ couple in the LiTFSI-EMSF electrolyte. The voltammogram for plating/stripping lithium on a platinum wire is shown in Fig. 1. The scan was started at 1.0 V *vs.* Li$^+$/Li and reversed at $-0.4$ V; the scan rate was 100 mV/s. The rise in cathodic current started at approximately $-0.2$ V *vs.* Li/Li$^+$ and was attributed to the reduction of lithium. The crossover of current after potential reversal was due to nucleation of the lithium, and surface area increases of the working electrode was changed. This might be caused by the first layer of plated lithium and/or the formation of lithium dendrites on the surface of the platinum substrate. Oxidation peaks were observed at 0.34 and 0.42 V; the first peak (0.34 V) is due to stripping of the plated lithium, and the second peak (0.42 V) is due to oxidation/extraction of lithium from Li-Pt alloys. The coulombic efficiency for the lithium redox reaction was 63%. Shi *et al.* discussed the Li-Pt alloys and reported low coulombic efficiency of lithium deposition/dissolution on platinum in the LiTFSI-ethylene carbonate/dimethyl carbonate electrolyte.[11] It was shown that a fraction of the Li-Pt alloys formed would not be available for stripping; this results in low coulombic efficiency in the first voltammetry scans. The initial scan, shown in Fig. 1, was the highest coulombic efficiency obtained. Subsequent scans exhibited progressively lower efficiencies.

Cyclic voltammetry (CV) experiments using the EQCN were used to measure the mass-to-charge for the insoluble electroactive species. The current density is given for its importance in battery applications. A voltammogram for the Pt quartz crystal in the LiTFSI-EMSF along with mass change is plotted in Fig. 2. The initial negative-going scan started at 2.0 V *vs.* Li/Li$^+$ and was reversed at $-0.4$ V. The shape of the current-voltage curve is similar to that shown in Fig. 1. Two oxidation peaks are located at 0.9 and 1.5 V (difference in potentials from Fig. 1 due to lack of IR compensation). The coulombic efficiency for the lithium redox reactions was 74%. The mass at the end of the oxidation portion of the CV was greater than the initial mass. The ratio of the mass lost during oxidation to the mass gained during reduction, mass efficiency, was 69%. Figure 2 compares the measured current density with the *rmc* from the EQCN. An effective equivalent weight of 8.5 was used in the calculation of *rmc* in Fig. 2. A close overlap of $dm/dt$ and current density was observed in the first 230 s, up to a potential of $-0.26$ V. It is possible that the underpotential deposition of lithium started at 1.15 V as a form of Li-Pt alloy and lasted until the scan reached $-0.26$ V. This coincides with the deposition of lithium metal without alloy formation at the more negative potentials. An overshoot of *rmc* was observed between 230 and 290 s, and the oxidation followed. Overshoot of *rmc* indicates that the effective equivalent weight is greater than 8.5. It suggests parasitic chemical reactions involving the electrodeposited lithium or the direct electroreduction of the electrolyte. The rising portion of the reduction peak showed no overshoot of the *rmc* curve because the reduced Li was in the form of a Li-Pt alloy, which has low reactivity with the electrolyte. But, at the most negative potential and the downhill portion of the reduction peak, an overshoot of the *rmc* curve was observed due to the reaction of the elemental Li deposited on the electrode. It has been reported that active lithium metal has a tendency to react with electrolytes and/or solvents to form a passivating layer.[9] There have been numerous publications about the formation of this protective layer with LiTFSI.[9,20]

Two chronoamperometry (CA) diagrams are shown in Fig. 3 and 4 with different reduction potentials, 0 and $-0.3$ V, respectively. The reduction was carried out for 80 s and followed by oxidation at 0.9 V. Lithium can be reduced to form Li-Pt alloys at 0 V (Fig. 3), and elemental lithium can be plated on the surface of the substrate at $-0.3$ V (Fig. 4) after the Pt electrode was saturated with Li-Pt alloys. Figure 3 shows that the *rmc* curve followed the current closely. An effective equivalent weight of 7.5 was used for the *rmc* calculation in both figures. During the oxidation step, an exact overlap of the *rmc* and current was observed, which indicates only lithium was electrochemically stripped.

The CA experiment at $-0.3$ V, Fig. 4, shows the reduction of lithium on the platinum electrode at a more negative potential. The increasing current during the constant potential reduction step im-

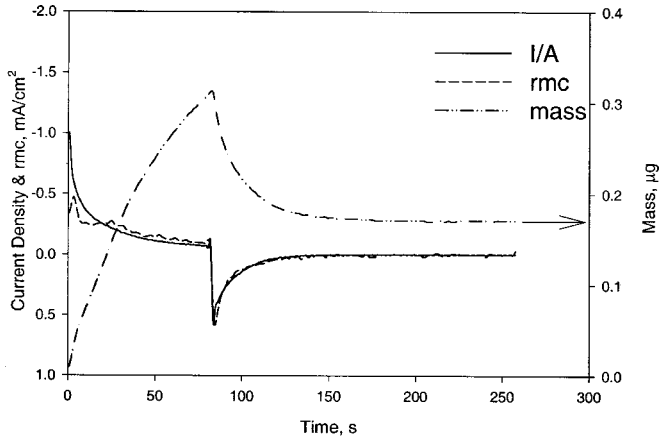


**Figure 3.** CA of platinum in LiTFSI-EMSF with mass change and *rmc*. Reduction potential was 0 V. Area of WE is 0.252 $cm^2$.

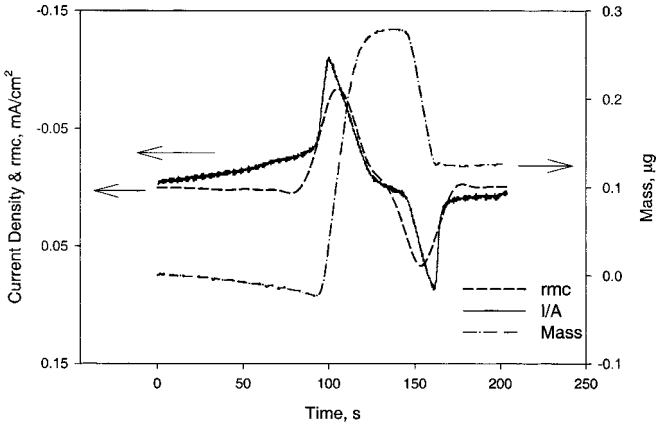


**Figure 5.** CV of aluminum in LiTFSI-EMSF with mass change and *rmc*. Switching potential was 0 V. Area of WE is 0.385 $cm^2$.

plies that elemental Li was deposited on the Pt surface with an increase in true area (constant superficial area), such as with rough or dendritic growth. The *rmc* curve in Fig. 4 is different from that in Fig. 3 at potentials between 0 and −0.3 V. Here, an effective equivalent weight of 11.0 was used in the *rmc* calculation. The *rmc* curve did not overlap the cathodic current, and its magnitude was much greater than the matching current; this indicates additional mass on the Li-plated electrode. The cause of this excess mass could be chemical reactions or electroreduction of the electrolyte. However, the *rmc* curve overlapped the current closely during the oxidation step; this showed that the decrease in mass on the electrode was mainly due to electro-oxidation.

Both CA experiments gave low coulombic and mass efficiencies. For Fig. 3, the coulombic and mass efficiencies are 42 and 47%, respectively; for Fig. 4, they are 50 and 44%. Varying the reduction potential improved the coulombic efficiency of the $Li^+$/Li couple but decreased the mass efficiency. These changes could be due to different forms of the reduced Li. The Li reduced at 0 V consisted mainly of Li-Pt alloys, but at −0.3 V, they were the sum of Li-Pt alloys and elemental Li on the surface. Poor reversibility of the $Li^+$/Li couple in the Li-Pt alloys is a possible cause of low coulombic efficiency in Fig. 3 (*i.e.*, extraction of the Li out of the alloy). This also contributed to the coulombic inefficiency in Fig. 4, but the chemical reactions between the reduced Li and the electrolyte would be the key cause of loss of charge. The *rmc* curve in Fig. 4 showed that lithium and other materials were plating on the electrode at more negative potentials. Products from these chemical reactions resulted in higher residual mass after the scan and lowered the mass efficiency for Fig. 4. These residual products were visually observed in the form of a black film.

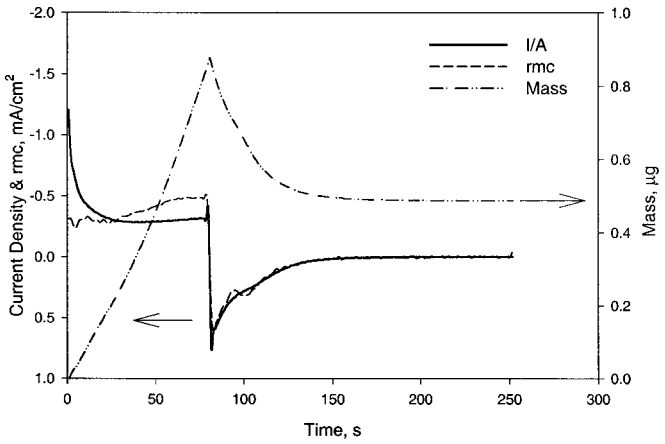


**Figure 4.** CA of platinum in LiTFSI-EMSF with mass change and *rmc*. Reduction potential was −0.3 V. Area of WE is 0.252 $cm^2$.

*Investigation of the Al substrate*.—Previous reports have discussed the formation of lithium-aluminum alloys by reduction of $Li^+$ from various solvents.[2,15,21] The relatively high coulombic efficiency for Li on an Al substrate has been shown to be due to the formation of Al-Li alloys.[2] The more positive reduction potential of the alloy than the pure metal lowers the chemical reactivity of Li with the electrolyte, producing ~95% coulombic efficiency.

A representative cyclic voltammogram of an Al wire (diam = 0.5 mm) in LiTFSI-EMSF is shown in Fig. 1 (dash = Al). The scan started at 1.2 V toward negative potentials and was reversed at −0.05 V. The coulombic efficiency for the lithium couple was 93%. A hysteresis in the current in Fig. 1 indicates changes made to the active surface area of the electrode during plating. Formation of Li-Al alloys probably caused these changes because the volume of Li-Al alloys is three times greater than that for Al. It is also possible that lithium was deposited on the electrode in the form of dendrites. Charge would be lost if these dendrites mechanically disconnected from the electrode, as suggested by others.[2,15] Figure 1 also compares the voltammograms of Li on the Al and Pt electrodes. There is a significant difference in the reduction potential of Li on the substrates. The Li reduction potential on the Al electrode was 0.3 V positive of that for the Pt substrate. The formation of the Li-Al alloy contributes to this shift in deposition potential. There was no second oxidation peak observed for the Al electrode. Only one of the Li-Al phases is reversible.

The mass change for an aluminum electrode in the LiTFSI-EMSF electrolyte was examined using the EQCN. Figure 5 shows results for an Al working electrode sputter-deposited on the Pt quartz crystal. The initial scan direction was toward negative potentials, and the switching potential was 0 V *vs.* $Li/Li^+$ which was reached at 100 s. A sharp rise of current at the 90 s mark is the start of lithium reduction, at which time the mass also increased. An oxidation current peak was observed at 160 s (0.6 V), and the mass on the electrode decreased simultaneously with current. However, some of the deposited mass remained on the electrode after the oxidation ended (51% mass efficiency). The coulombic efficiency was also low at 67%. This low coulombic efficiency for the Al on the quartz crystal is due to structural damage on the thin aluminum film electrode.[15] Some of Li-Al alloys were not recoverable and fell off the electrode during the cycle.

The rate of mass change was also plotted along with the current in Fig. 5 to examine the mass change on the electrode. Effective equivalent weights of 36 for reduction and 28 for oxidation were

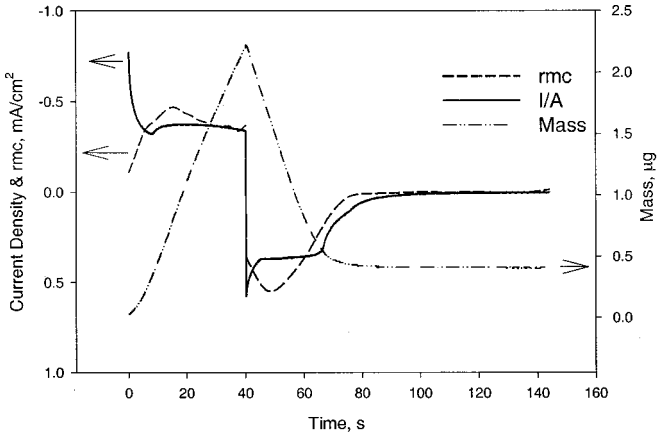


**Figure 6.** CA of aluminum in LiTFSI-EMSF with mass change and *rmc*. Area of WE is 0.385 cm$^2$.

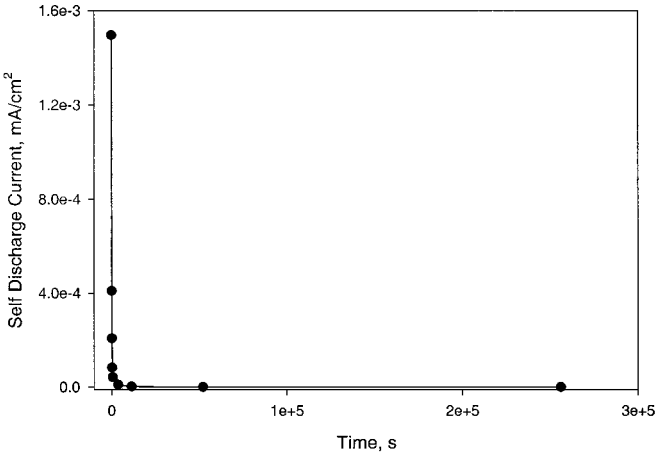


**Figure 7.** Self-discharge rate of lithium on aluminum substrate.

used to calculate *rmc*. The shape of the *rmc* curve was somewhat similar to the current density curve, but the positions of the reduction and oxidation peaks for the current density and the *rmc* curves were different. Based on the *rmc* curve, most of the lithium deposition occurs after the scan was reversed, and most of mass was stripped before the current reached the oxidation peak. The high equivalent weights suggest that products other than lithium were deposited on the electrode. This was also shown earlier for the Pt electrode at more negative potentials, but the equivalent weight values of these products in Fig. 5 were higher (36) than ones calculated for the Pt electrode (11). High equivalent weight values indicate that this film is thicker than ones found around the Pt electrode at the fixed electrode area. This film acts as a passivating layer and protects the remaining Li-Al alloys from further chemical reactions. EMSF would be one possible component to react with the plated lithium to form the passivating film. This anion shows reactivity towards lithium metal, along with other typical lithium anions used in other Li battery studies.[10]

The passivating film was also shown as the cause of the mass difference after the cycle. The mass on the electrode of the quartz crystal at the end of the scan was greater than the initial mass. This residual mass is likely the remaining passivating film because its magnitude is greater than the unoxidized Li (based on the coulombic efficiency). However, another factor that affects the residual mass is the mechanical integrity of the Li-Al alloy. It was visually observed that the Al film on the Pt quartz crystal partially peeled off from the substrate due to the structural stress of the Li-Al alloys on the elemental Al. It is possible that mechanical detachment of products or Li-Al alloys coincided with the Li oxidation process. Thus, the residual mass is the amount of the remaining passivating film. Quantitative assessment of these simultaneous processes is not possible without further experimental information.

A CA experiment with the EQCN for $Li^+$/Li on the Al-Pt quartz crystal is plotted in Fig. 6. The reduction potential was $-0.3$ V, and the stripping potential was 1.2 V. When the potential step was changed to 1.2 V, where oxidation occurred, a drop in current was observed. The coulombic and mass efficiencies in Fig. 6 were both 83%. The effective equivalent weight was 36.5 and used to calculate the *rmc*, which was also plotted in Fig. 6. This value indicates that a passivating film formed as Li was reduced. The higher coulombic efficiencies for Fig. 6 were due to the stability of the Li-Al alloys on the electrode. Again, the oxidation part of *rmc* peaked earlier than the oxidation current; this was because the actual mass includes loss of Li-Al alloys and the passivating film, coinciding with electrooxidation of Li. For Fig. 6, the amount of Li-Al alloy loss was less than the loss of Li-Al alloy in Fig. 5.

The self-discharge current for the $Li^+$/Li couple was measured by performing chronopotentiometry, as shown in Fig. 7. Lithium was plated at constant current for 300 s; then the system was held in open-circuit for varying time periods. The time was changed from 30 s to 3 days, followed by a constant-current oxidation step. From Fig. 7, most of the charge loss occurred in the beginning of the open-circuit period. The effective rate of self-discharge of lithium in the LiTFSI electrolyte calculated from the 3 day open-circuit test was 0.3 µA/cm$^2$. This is about 70 times lower than sodium in a 1,3 methylpropyl imidazolium melt, *i.e.*, 22 µA/cm$^2$.[22] The estimated weight of the protective film was 9.4 µg, assuming EMSF and lithium are the only components of the film. The total mass of lithium deposited was 7 µg. This agreed with the earlier experiment, which showed that the protective layers formed as lithium was deposited. These layers constitute the nonrecoverable charge but prevent further chemical reaction of the lithium with the electrolyte. On Pt, the open-circuit tests showed 0% recovery of charge after a 30 s open-circuit period.

*Investigation on the mercury electrode.*—A mercury film electrode was used in CV scans to investigate the potential dependence of the $Li^+$/Li couple. Figure 8 shows the voltammogram for LiTFSI

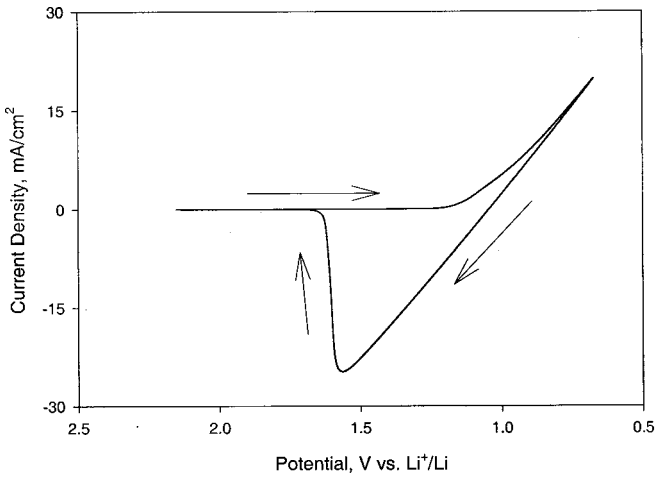


**Figure 8.** CV of Hg electrode in LiTFSI-EMSF. Area of WE is 0.318 cm$^2$.

in an EMSF melt on the mercury film electrode. The reduction potential for lithium on the Hg film electrode is 1 V more positive than on platinum. The reduction for $Li^+$ started at 1.2 V *vs.* $Li^+/Li$. A hysteresis in the current was not observed because it forms an amalgam with Hg. The coulombic efficiency of this CV scan was 99%, and the maximum current density was approximately 20 $mA/cm^2$, which is three times larger than that obtained using the aluminum substrate, due to the absence of film formation.

Chronoamperometry of the LiTFSI-EMSF electrolyte on a mercury film electrode was performed. Plating and stripping times were 1 h each. Coulombic efficiency of the lithium redox reaction was 99%. The cathodic current fluctuated in the first 1500 s but dropped to near-zero at 2000 s. This current drop is due to saturation of the mercury film electrode with Li-Hg alloys. Near-100% coulombic efficiency for $Li^+/Li$ couple on the Hg film electrode was achieved because the Hg film electrode provides a more positive reduction potential by forming Li-Hg alloys.

A comparison of the results for Pt, Al, and Hg electrodes suggests that the reduction potential is the critical parameter in the electrochemical stability of Li in the LiTFSI-EMSF electrolyte. Chemical reactions of the lithium and electrolyte contribute to the efficiency loss with the Pt and Al electrodes. The reduction potential is inversely proportional to the free energy. For Pt, the reduction potential for the Li couple was the most negative among the three metal electrodes; it showed the lowest coulombic efficiency. The reduction potential for the Al electrode was between those of Pt and Hg, providing $>90\%$ coulombic efficiency. Approximately 7% of the Li-Al alloy reacted with the electrolyte, and these products acted as protective films on the surface of the Li-Al alloy.

## Conclusions

Results from cyclic voltammetry, chronoamperommetry, and electrochemical quartz crystal microbalance experiments show that the LiTFSI-EMSF electrolyte has high conductivity and can accommodate the lithium redox couple as an anode. Reactivity of the electrolyte towards metallic lithium still exists in this electrolyte, but the formation of lithium-metal alloys suppresses this reactivity. Coulombic efficiency of the $Li^+/Li$ couple on these electrode materials approached 100% as the reduction potential shifted to positive values because of the lowered free energy of the alloys. High coulombic efficiencies for the Li redox couple were obtained only on the Al and Hg substrates, which form Li-Al and Li-Hg alloys.

## Acknowledgments

This project was supported by the U.S. Department of Energy, Basic Energy Science, under grant no. DE-FG02-97ER14798. In particular, Dr. Paul Maupin, Program Manager, is gratefully acknowledged for his support and encouragement.

We would like to give special thanks to Jim O'Connor and Mike Matson at Phillips Research Center for ethyl methyl sulfone and their technical support, Steven Boyd at 3M for the donation of lithium bis(trifluoromethanesulfonyl)imide, and Professor C. A. Angell, Department of Chemistry, Arizona State University, for his technical assistance on ethyl methyl sulfone.

We would also like to give special thanks to Ravindra Tanikella for preparing Al electrodes on the Pt quartz crystal.

*Georgia Institute of Technology assisted in meeting the publication costs of this article.*

## References

1. S. Machill and D. Rahner, *J. Power Sources*, **54**, 428 (1995).
2. A. S. Baranski and W. R. Fawcett, *J. Electrochem. Soc.*, **129**, 901 (1982).
3. H. Yang, K. Kwon, T. M. Devine, and J. W. Evans, *J. Electrochem. Soc.*, **147**, 4399 (2000).
4. K. Xu, S. Zhang, and C. A. Angell, *J. Electrochem. Soc.*, **143**, 3548 (1996).
5. J. Fuller, R. A. Osteryoung, and R. T. Carlin, *J. Electrochem. Soc.*, **142**, 3632 (1995).
6. D. Aurbach and A. Zaban, *J. Electroanal. Chem.*, **393**, 43 (1995).
7. K. Xu and C. A. Angell, *J. Electrochem. Soc.*, **145**, L70 (1998).
8. Y. Matsuda, M. Morita, and M. Ishikawa, *J. Power Sources*, **68**, 30 (1997).
9. D. Aurbach, Y. Gofer, A. Schechter, O. Chusid, H. Gizbar, Y. Cohen, M. Moshkovich, and R. Turgeman, *J. Power Sources*, **97-98**, 269 (2001).
10. D. R. McFarlane, J. Sun, J. Golding, P. Meakin, and M. Forsyth, *Electrochim. Acta*, **45**, 1271 (2000).
11. Z. Shi, M. Liu, D. Naik, and J. L. Gole, *J. Power Sources*, **92**, 70 (2001).
12. H. Yang, K. Kwon, T. M. Devine, and J. W. Evans, *J. Electrochem. Soc.*, **147**, 4399 (2000).
13. Z. Liu and J. Y. Lee, *J. Power Sources*, **97-98**, 247 (2001).
14. M. Mohamedi, S.-J. Lee, D. Takahashi, M. Nishizawa, T. Itoh, and I. Uchida, *Electrochim. Acta*, **46**, 1161 (2001).
15. Y. Hamon, T. Brousse, F. Jousse, P. Topart, P. Buvat, and D. M. Schleich, *J. Power Sources*, **97-98**, 185 (2001).
16. Z. Lin, C. M. Yip, I. S. Joseph, and M. D. Ward, *Anal. Chem.*, **65**, 1546 (1993).
17. K. K. Kanazawa and O. R. Melroy, *IBM J. Res. Dev.*, **37**, 157 (1993).
18. J. Rickert and A. Brecht, *Anal. Chem.*, **69**, 1441 (1997).
19. M. Urbakh and L. Daikhin, *Colloids Surf., A*, **134**, 75 (1998).
20. J.-Y. Sanchez, F. Alloin, D. Benrabah, and R. Arnaud, *J. Power Sources*, **68**, 43 (1997).
21. S. Biallozor and M. Lieder, *J. Electrochem. Soc.*, **140**, 2537 (1993).
22. G. E. Gray, P. A. Kohl, and J. Winnick, *J. Electrochem. Soc.*, **143**, 3820 (1996).